Thin Solid Films 518 (2010) 7147–7151

Contents lists available at ScienceDirect

Thin Solid Films

journal homepage: www.elsevier.com/locate/tsf

Charge recombination reduction in dye-sensitized solar cells by means of an electron beam-deposited TiO_2 buffer layer between conductive glass and photoelectrode

Michele Manca [a,*], Francesco Malara [b], Luigi Martiradonna [a], Luisa De Marco [a], Roberto Giannuzzi [b], Roberto Cingolani [a], Giuseppe Gigli [a]

[a] Italian Institute of Technology (IIT), Center for Bio-Molecular Nanotechnology, Via Barsanti, 1 Arnesano (Le) 73010, Italy
[b] National Nanotechnology Laboratory (NNL) of CNR-Istituto di Nanoscienze, Distretto Tecnologico, Università del Salento, Via Arnesano 16, Lecce 73100, Italy

ARTICLE INFO

Article history:
Received 3 November 2009
Received in revised form 1 July 2010
Accepted 9 July 2010
Available online 16 July 2010

Keywords:
Titanium dioxide
Dye solar cells
Electron beam evaporation
Buffer layer
Recombination

ABSTRACT

A thin anatase titanium dioxide compact film was deposited by electron beam evaporation as buffer layer between the conductive transparent electrode and the porous TiO_2-based photoelectrode in dye-sensitized solar cells. The effect of such a buffer layer on the back transfer reaction of electrons to tri-iodide ions in liquid electrolyte-based cells has been studied by means of both electrochemical impedance spectroscopy and open circuit photovoltage decay analysis. The influence of the thickness has been also investigated and an increment in overall quantum conversion efficiency η as high as +31% with respect to the standard cell – fabricated onto an uncoated conductive glass – has been revealed in the case of a 120 nm thick buffer layer.

1. Introduction

Solar cells based on dye-sensitization of mesoporous TiO_2 electrodes (DSSCs) are regarded as a low-cost and high efficiency alternative to conventional photovoltaic devices [1–12]. DSSCs consist of a monolayer of a photosensitizing dye adsorbed on a mesoporous film of nanocrystalline oxide semiconductors, typically anatase titanium dioxide. Dye molecules are chemisorbed through functional anchoring groups on the surface of the semiconductor, while the pores of the film are generally filled with a iodide/tri-iodide electrolyte. When an incident photon excites the dye, this injects an electron into the conduction band of the semiconductor. Positively charged dyes are then reduced by the iodide species I^- and the electrical circuit is completed by the reduction of I_3^- at the platinum counter electrode.

Although intensive research efforts have been so far focused on DSSCs, there are still several factors limiting the efficiency of such devices; among them the recombination of photogenerated carriers is one of the most important. Recombination in DSSCs is primarily an interfacial process, in contrast to the bulk process that occurs in conventional p–n junction solar cells. In principle, therefore, interfacial engineering, rather than improved materials quality, may be used to decrease the recombination rate in dye-sensitized nanoporous films. There are basically two routes for electron transfer to redox ions in the electrolyte: via the nanocrystalline TiO_2 and via the F:SnO_2 substrate (FTO). Electron transfer via both the routes needs to be minimized in order to prevent the loss of photoinjected electrons by back reaction [13]. The energy-wasting pathway considered in this work is the recombination of the electrons in the FTO substrate, e_{FTO}, with the oxidized redox species of the electrolyte

$$e_{FTO} + R^+ \rightarrow R.$$

This reaction occurs because the nanocrystalline TiO_2 does not completely cover the SnO_2 substrate; there are numerous spaces between the colloidal particles where the substrate comes into direct contact with the redox solution [14,15]. Its results are favored by the high concentration of electrons in the degenerately doped SnO_2 relative to the TiO_2.

Recently, many researchers have paid attention to the interface of FTO/TiO_2 [16,17]. It is reported that electrons must be extracted efficiently from the nanocrystalline TiO_2 layer, but transfer of electrons to the electrolyte phase should be inhibited [18]. An addition of 4-tert-butylpyridine into electrolyte solution is a well known method to prevent the carrier leakage of direct electron acceptance from the nanocrystalline TiO_2 film with avoidance of hole mediation to optically excited dye [19]. The TiO_2 thin layer coated directly on to the FTO glass substrate, applied by spray pyrolysis technique [20], has been found to prevent the back transfer of electrons to the electrolyte from the FTO substrate. The use of a phenol/2-allyphenol copolymer applied by electrodeposition [21] and sol–gel derived thin TiO_2 film [22] as a blocking (passivating) layer has also been investigated. Some researchers tried to prepare thin

* Corresponding author. Tel.: +39 0832 298375; fax: +39 0832 298237.
E-mail address: michele.manca@iit.it (M. Manca).

0040-6090/$ – see front matter
doi:10.1016/j.tsf.2010.07.047

TiO_2 blocking layer by dry processes such as sputtering method [23,24] and chemical vapor deposition method [25], which are suitable for forming uniform and fine membrane over large areas with material properties more stable than the wet process. Xia et al. recently used a thin Nb_2O_5 film deposited by two different techniques [26,27] as a blocking layer between FTO and TiO_2 nanocrystalline: they demonstrated an improvement in V_{OC} of about 70 mV and an overall energy conversion efficiency which was 20% higher than that of the unblocked device.

In this study, we investigated the recombination blocking effect due to the introduction of a thin TiO_2 anatase buffer layer (BL) deposited by electron beam evaporation (EBE) at the interface between conductive glass and mesoporous photoelectrode. Compared to other deposition techniques, the EBE system has some advantages, such as high deposition efficiency, deposition free from the plasma damage caused by γ electrons, O^- ions and high atomic mobility at the surface of the substrate [28–30].

The improvement of the DSSC performances has been evaluated for different buffer layer thicknesses and a critical analysis of the charge-transfer phenomena laying on the basis of such an improvement has been carried out by means of either electrochemical impedance spectroscopy (EIS) and open circuit photovoltage decay (OCVD) measurements.

2. Experimental details

2.1. Deposition of TiO_2 buffer layers by means of electron beam evaporation

20×20 mm^2 FTO-coated glass samples (Solaronix, 10 Ω/sq) were inserted in an high electron beam evaporation chamber, 60 cm far from a water-cooled crucible containing TiO_2 tablets bought from Umicore. After vacuuming the chamber at 10^{-6} mbar, an overflow of oxygen (10 sccm) was introduced to preserve the stoichiometry of the deposited layers. The chamber was also heated through two tungsten lamps, whose power was controlled through a feedback circuit in order to maintain the evaporation temperature fixed. The TiO_2 target was heated through a Temescal Supersource electron gun. Both evaporation rate and chamber temperature were optimized in order to obtain low surface roughness and a high crystalline quality after the sintering cycle (up to 520 °C) in an oven. Several thicknesses ranging from 20 nm to 200 nm were also tested aiming to optimize the final performances of the solar cells.

2.2. DSSC fabrication

Having cleaned the FTO-coated glass samples with a detergent solution using an ultrasonic bath for 15 min and washed them with water and ethanol, a commercial P25(Degussa)-based TiO_2 paste was prepared according the reported literature [19] and then deposited onto the conducting glasses by screen-printing (screen characteristic: polyester, mesh count, 200 mesh/cm; mesh opening 60 μm) and dried at 130 °C for 6 min; this procedure was repeated several times in order to obtain the wanted film thickness. The film thickness and the dimensions of the active area were measured using the profilometer. The electrodes coated with the TiO_2 pastes were gradually heated under air flow at 325 °C for 5 min, at 375 °C for 5 min, at 450 °C for 15 min, and at 500 °C for 15 min. In Fig. 1 we report the SEM micrographs of a such treated film.

After cooling to 80 °C, the TiO_2 electrodes were immersed into a solution of 0.5 mM (bis(tetrabutylammonium)-cis-di(thiocyanato)-N, N′-bis(4-carboxylato-4′-carboxylic acid-2, 2-bipyridine) ruthenium(II) (N719) in a mixture of acetonitrile and tert-butyl alcohol (v/v, 1:1), and kept at room temperature for 14 h.

The solar cells were assembled by placing a platinum-coated conducting glass (counter-electrode) on the N719 dye-sensitized photoelectrode (working electrode). The two electrodes were assembled into a sandwich type cell and sealed with a Surlyn hot-melt gasket 30 μm thick. The redox electrolyte was introduced into the space of inter-electrodes through the hole pre-drilled on the back of the counter-electrode. The holes were sealed up using Surlyn hot-melt film and a cover glass. The redox electrolyte used was 0.1 M LiI, 0.05 M I_2, 0.6 M 1-methyl-3-propylimidazolium iodide, and 0.5 M tert-butylpyridine in dried acetonitrile.

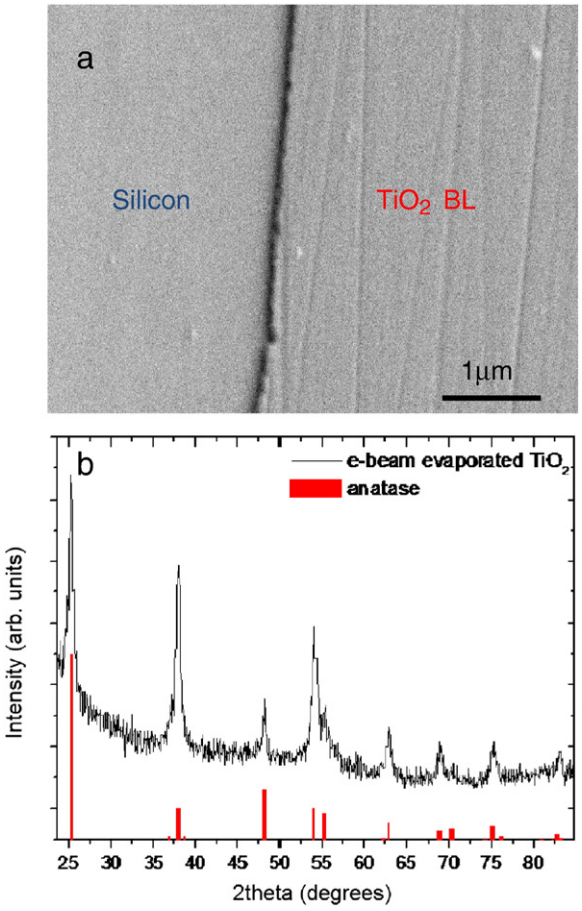

Fig. 1. a) SEM image showing the border of a 200 nm thick TiO_2 buffer layer deposited by e-beam evaporation on Si substrate and annealed at 520 °C; b) X-ray diffraction pattern of the same film (black curve). Red bars indicate the expected position of anatase phase diffraction peaks.

2.3. Characterization

The thickness of the transparent films was measured with Tencor Alpha-Step 500 Surface Profiler. A Varian Cary 5000 UV–Vis Spectrophotometer was used to measure the UV–Vis absorption spectra of the as prepared films and the desorption solutions.

SEM characterization of TiO_2 photoelectrode morphology was performed with a RAITH 150 EBL instrument.

X-ray diffraction (XRD) patterns were collected through an X'PERT PRO Diffractometer (Panalytical), using Cu-Kα radiation supplied with 45 kV and 40 mA.

Photocurrent–voltage I–V measurements were performed using a Keithley unit (Model 2400 Source Meter). A Newport AM 1.5 Solar Simulator (Model 91160A equipped with a 300 W Xenon Arc Lamp) served as a light source, and its light intensity (or radiant power) was calibrated to 100 mW/cm^2 using a reference a Si solar cell. The light source for the incident photon-to-current conversion efficiency (IPCE) measurements was the Solar Simulator equipped with a Spectral Products monochromator (Model CM110 1/8 m). The intensity was

measured with Newport Radiant Power Meter (Model 70260 combined with the 70268 Probe) and a UDT Instrument Model 221 calibrated photodiode. Three parallel samples for each kind of layer structure were made for current–density vs photovoltage (J–V) and IPCE measurement, and the reproducibility of TiO_2 photoelectrodes was quite good.

Electrochemical impedance spectroscopy (EIS) spectra have been measured by using an AUTOLAB PGSTAT 100 potentiostat operating in two-electrode mode. Measurements have been carried out under dark condition at open circuit potential: frequency range 300 kHz–30mHz; AC voltage 10 mV. The frequency-dependent impedance was fitted by using the EC-LAB software (from Bio-LOGIC SAS) with the aim to obtain the space charge capacitance of the uncoated and TiO_2-coated FTO electrodes. The dependence of the photovoltage on intensity was determined by illuminating the cells with a green light emitting diode ($\lambda = 532$ nm).

3. Results and discussion

3.1. Morphology and crystallinity of the electron beam evaporated TiO_2 buffer layers

Electron beam evaporated TiO_2 layers were contemporaneously deposited on glass substrates and on miscut-Si for XRD characterization. Several deposition rates and evaporation temperatures were tested, in order to optimize both the surface roughness and the crystal structure. It has been observed that deposition rates higher than 2 A/s led to a significant increase of roughness in films thicker than 100 nm. Therefore, the evaporation rate was cautiously fixed at 1.5 A/s. Similarly, chamber temperatures ranging from 200 °C to 260 °C were tested. Although the crystal structure of as-deposited layers revealed to be amorphous with XRD analysis, after an annealing step at 520 °C typical sharp peaks of TiO_2 anatase phase could be identified in the diffraction spectrum of films deposited at temperatures higher than 230 °C. Fig. 1 shows a typical diffraction pattern (black line) collected from a 100 nm thick TiO_2 layer deposited at 260 °C and annealed at 520 °C. The direct comparison with the expected diffraction pattern of TiO_2 anatase (red bars) clearly indicate the presence of a single phase in the realized patterns. The same deposition (260 °C, 1.5 A/s) and annealing conditions were therefore exploited for the deposition of several films on FTO-coated substrates with thicknesses ranging from 20 nm to 200 nm.

3.2. Effect of the TiO_2 buffer layer on the performances of a DSSC

The correlation between the presence of the TiO_2 BL and the DSSC performances has been investigated with the aim to find the optimum thickness in order to minimize the recombination effects as well as to improve the injection of the photogenerated electrons in the TCO layer. The J–V curves for the four DSSCs with electron beam evaporated TiO_2 buffer layers having 20 nm, 50 nm, 120 nm and 200 nm thicknesses are shown in Fig. 2 in comparison to a cell fabricated on an uncoated TCO substrate (reference), while a resume of their photovoltaic characteristics is reported in Table 1. Both the short-circuit photocurrent density J_{SC} and the open circuit voltage V_{OC}, showed a growing trend. J_{SC} rose from 11.24 mA/cm^2 – corresponding to the uncoated TCO – up to a 14.33 mA/cm^2 value achieved with a 120 nm thick BL; a further increment of the thickness didn't turned into an increment of photocurrent density. V_{OC} showed instead a conspicuous enhancement – up to a value of 0.76 V – also in the case of the 200 nm thick buffer layer. As a result, the highest increment in overall quantum conversion efficiency η, consisting in a +31% respect to the standard uncoated TCO-based cell, has been revealed with a 120 nm thick BL. This result is well consistent with the hypothesis that, under open circuit illumination conditions, the Fermi level of the FTO substrate typically rises by up to 0.7 eV, so that to produce a much larger driving force for electron transfer from the FTO to I_3^- [13]. Under these conditions, the back reaction of electrons with I^{3-} via the FTO strongly affect the performances of the cell and it cannot be neglected.

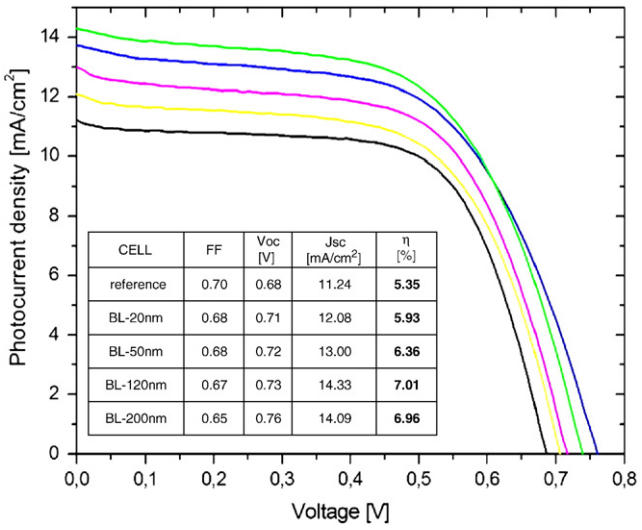

CELL	FF	Voc [V]	Jsc [mA/cm^2]	η [%]
reference	0.70	0.68	11.24	**5.35**
BL-20nm	0.68	0.71	12.08	**5.93**
BL-50nm	0.68	0.72	13.00	**6.36**
BL-120nm	0.67	0.73	14.33	**7.01**
BL-200nm	0.65	0.76	14.09	**6.96**

Fig. 2. J–V curve of DSSCs made on TCO coated with BL having different thicknesses.

3.3. EIS analysis

Electrochemical impedance spectroscopy (EIS) is the most effective technique to investigate the charge transport phenomena in a DSSC [36].

Fig. 4 shows the EIS spectra measured in dark condition at a potential corresponding to the value of open circuit state under 1 sun illumination and plotted in a Nyquist diagram for a frequency range comprised between 30 mHz and 100 kHz. The main contribution to the first (high frequency) arc arises from the parallel connection of the coupling between the Helmholtz capacities of both electrodes and the charge-transfer resistance at the TCO/photoelectrode interface [31,32], whereas the charge-transfer resistance of the platinized TCO counter-electrode is considered to be relatively small as it presents little changes with potential in comparison to bare TCO [35]. The second (intermediate frequency) arc corresponds to electron transfer resistance from the dye-sensitized nanocrystalline TiO_2 film to the electrolyte as well as to the back reaction of electrons with I_3^- via the FTO. The third (low frequency) arc – corresponding to the diffusion of I_3^- (holes) in the electrolyte – has not been evidently detected here. The general equivalent circuit of a DSSC presented by Fabregat-Santiago et al. [35], is illustrated in Fig. 3.

In Fig. 4a a significant reduction of the higher-frequencies arc size in the cells with BL can be observed, this attesting an overall reduction of the charge injection barrier in correspondence of the blue-highlighted interface in the schematic representation reported in Fig. 3.

For fitting the experimental data, the equivalent circuit proposed by Wang et al. [33] for the case of cells exhibiting a good carrier collection efficiency was used. Constant phase elements have been used instead of pure capacitors as they better describe the uneven and

Table 1
Fitted parameters from the Wang et al. [33] equivalent circuit.

CELL	R_{CO+CE} [Ω]	C_{CO+CE} [μF]	a_{CO+CE}	R_{CT} [Ω]	C_{CT} [μF]	a_{CT}
Reference	23	64	0.72	197	107	1
BL-20 nm	5.6	238	0.69	118.2	217	0.98
BL-50 nm	4.4	494	0.58	99.3	262	0.98
BL-120 nm	6.1	1634	0.46	73.2	359	0.99
BL-200 nm	3.3	1589	0.49	91.7	304	0.98

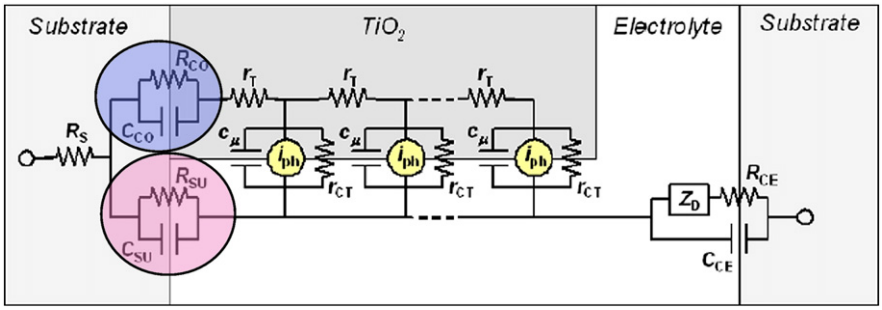

Fig. 3. General equivalent circuit model of a DSSC. The r_{CT} is the charge-transfer resistance of the charge recombination process between photogenerated electrons and I_3^- in electrolyte; c_μ is the chemical capacitance of TiO_2 film; Z_D is the Warburg element showing the Nernst diffusion of I_3^- in electrolyte; R_{CE} and C_{CE} are the charge-transfer resistance and double-layer capacitance at the counter-electrode (platinized TCO glass); R_{SU} and C_{SU} are the charge-transfer resistance and the corresponding double-layer capacitance at exposed TCO/electrolyte interface; R_{CO} and C_{CO} are the resistance and the capacitance at TCO/TiO_2 contact; Rs is the series resistance, including the sheet resistance of TCO glass and contact resistance of the cell.

porous electrodes. In Table 1 we reported the extrapolated values of the most characteristic elements of the transmission line:

- series charge-transfer resistance $R_{CO} + R_{CE}$
- series double-layer capacitance C_{CO+CE} and its correspondent capacitor ideality's coefficient a_{CO+CE}
- transfer resistance of the charge recombination processes both at titania/dye/electrolyte and FTO/electrolyte interfaces R_{CT} ($= r_{CT}/L$, where L is the thickness of the nanoporous TiO_2 film)

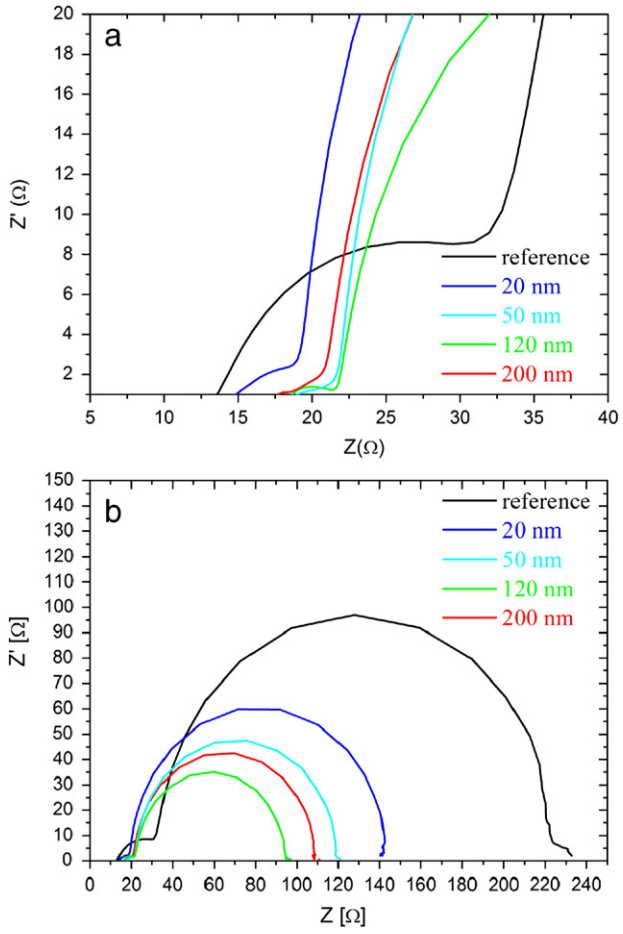

Fig. 4. Impedance spectra of DSSCs made on TCO coated with BL having different thicknesses. Measurements carried out in dark condition at a potential corresponding to the value of open circuit state under 1 sun illumination; frequency range of 100 kHz–30 m Hz; AC voltage 10 mV.

- chemical capacitance of the charge recombination processes both at titania/dye/electrolyte and FTO/electrolyte interfaces C_{CT} ($= c_\mu L$, where L is the thickness of the nanoporous TiO_2 film) and its capacitor ideality's coefficient a_{CT}.

Passing from the uncoated to the BL-coated photoelectrode, the charge-transfer resistance R_{CO+CE} – calculated as the sum of the component associated to the photoelectrode/TCO interface and the one associated to the electrolyte/platinum interface respectively – resulted to be reduced by about a factor 5 as a consequence of an improvement of the electrical contact mostly arising from the better adherence of the evaporated compact layers. As a secondary effect, the coated electrodes exhibit also a remarkably more intense capacitive behavior. The increase of the capacitance at TCO/photoelectrode interface C_{CO} is related to the presence of the buffer layer that reduces the back recombination from the FTO electrons and promotes a larger charge accumulation at the interface and hence an increment in V_{OC} [36]. The V_{OC} of a DSSC corresponds to the difference between the quasi-Fermi level of the TiO_2 porous film under illumination and the redox potential of the electrolyte. The accumulation of photogenerated electrons results in a higher quasi-Fermi level, this being in perfect accordance with the growth of the C_{CO+CE} for cells based on ticker BLs.

Concerning the second semicircle, a strong reduction of transfer resistance of the charge recombination processes – that in the case of the abovementioned experimental conditions is exclusively related to the reduction of the resistance R_{SU} at the TCO/electrolyte interface (the pink-highlight in the schematic representation reported in Fig. 3) – was also observed: R_{CT} fell down from 197 Ω for a cell made on the uncoated-FTO to 73.2 Ω for a cell with a 120 nm thick EB-evaporated blocking layer. In fact, at applied potentials more negative than about −0.4 V, the buffer layer becomes sufficiently conductive so that electron transfer from the FTO-coated substrate to I_3^- becomes easier [36]. Under this condition, electron transfer from the FTO substrate to I_3^- becomes easy, leading to a fast decrease of R_{CT} [36].

Even in this case the coated samples show an increase of the chemical capacitance related to a larger charge accumulation at the FTO/electrolyte interface.

3.4. OCVD analysis

OCVD analysis has been conducted by monitoring the subsequent decay of open circuit voltage after stopping the illumination on DSSC under open circuit conditions [34]. By means of this technique, the gradual loss of photogenerated electrons due to recombination can be monitored by measuring the transient decay of the cell voltage after switching off the light. The decay of the photovoltage reflects the decrease of the electron concentration at the FTO surface, which is mainly caused by charge recombination. This means that the

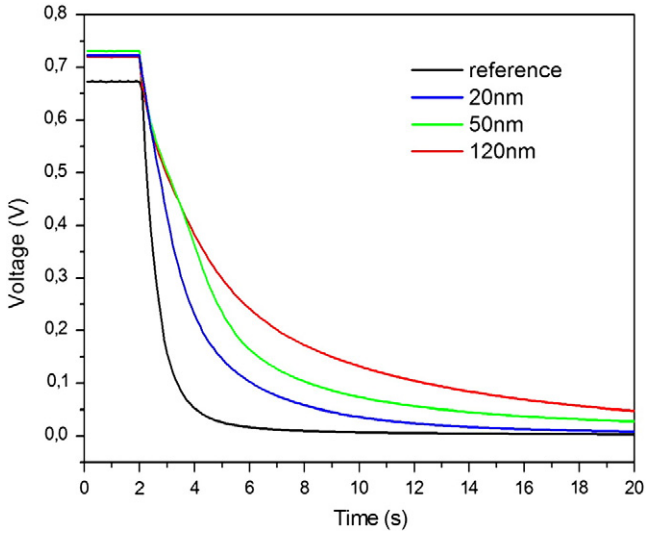

Fig. 5. OCVD curves for DSSCs with 0 (reference), 20, 50, and 120 nm thick buffer layers.

recombination velocity of photoelectron is proportional to the response of the OCVD. Fig. 5 shows the OCVD curve for DSSC having respectively 0 (reference), 20, 50 and 120 nm thick buffer layers.

The BLs strongly influence the slow decay component of the photovoltage decay, whereas the initial rapid decay of the photovoltage is much less sensitive to their presence. This indicates that the transfer of electrons responsible for the lowering of the quasi-Fermi level in a cell without a blocking layer occurs at least partly via the exposed FTO substrate and that the decay of the photovoltage reflects the decrease in the concentration of electrons in the conduction band of the nanocrystalline TiO_2 particles immediately adjacent to the substrate contact [13].

As a consequence of such a slower decay, a sensible increase in electron life-time can be demonstrated for the BL-based cells, since the reduction of the charge recombination resistance R_{CT} is compensated by a sensitively higher capacitance C_{TCO}.

4. Conclusions

Thin anatase TiO_2 buffer layers were deposited by electron beam evaporation between TCO and porous TiO_2-based photoelectrode in DSSCs and their electrochemical characteristics were examined either by EIS or OCVD analysis. The improvement of the photovoltaic performances has been evaluated for different buffer layer thicknesses. V_{OC} showed a conspicuous enhancement passing from 0.68 V for an uncoated TCO-based cell to 0.76 V for a substrate coated with a 200 nm thick BL, whereas the highest relative increment in overall quantum conversion efficiency η, consisting in +31%, was revealed with a 120 nm thick BL.

Acknowledgements

This work has been partially supported by DAUNIA SOLAR CELL c/o TRE-TOZZI RENEWABLE ENERGY group as an industrial partner. The authors would like to thank Paola Pareo for the SEM images, Giacomo Gorni, Francesco Matteucci, Valerio Borzatta, Francesca Martina, Silvio Pappadà (cuscinusa sape) and Fabio Morrison for beneficial discussions.

References

[1] B. O'Regan, M. Gratzel, Nature 353 (1991) 737.
[2] Q. Wei, K. Hirota, K. Tajima, K. Hashimoto, Chem. Mater. 18 (2006) 5080.
[3] B. Tan, Y. Wu, J. Phys. Chem. B 110 (2006) 15932.
[4] B. Liu, E.S. Aydil, J. Am. Chem. Soc. 131 (2009) 3985.
[5] R.R. Bacsa, J. Dexpert-Ghys, M. Verelst, A. Falqui, B. Machado, W.S. Bacsa, P. Chen, S.M. Zakeeruddin, M. Graetzel, P. Serp, Adv. Funct. Mater. 19 (2009) 875.
[6] M.K. Nazzerruddin, A. Kay, I. Rodicio, R. Humphy-Baker, E. Muller, P. Liska, N. Vlachopoulos, M. Gratzel, J. Am. Chem. Soc. 115 (1993) 6382.
[7] K. Kalyansundaram, M. Gratzel, Coord. Chem. Rev. 77 (1998) 347.
[8] U. Bach, D. Lupo, P. Comte, J.E. Moser, F. Weissörtel, J. Salbeck, H. Spreitzer, M. Gratzel, Nature 395 (1998) 583.
[9] S. Kambe, K. Murakoshi, T. Kitamura, Y. Wada, S. Yanagida, H. Kominami, Y. Kera, Sol. Energy Mater. Sol. Cells 61 (2000) 427.
[10] Z.S. Wang, H. Kawauchi, T. Kashima, H. Arakawa, Coord. Chem. Rev. 248 (2004) 1381.
[11] D.S. Tsoukleris, I.M. Arabatzis, E. Chatzivasiloglou, A.I. Kontos, V. Belessi, M.C. Bernard, P. Falaras, Sol. Energy 79 (2005) 422.
[12] S. Ito, P. Chen, P. Comte, M.K. Nazzeruddin, P. Liska, P. Pechy, M. Gratzel, Prog. Photov. Res. Appl. 15 (2007) 603.
[13] P.J. Cameron, L.M. Peter, J. Phys. Chem. B 107 (2003) 14394.
[14] A. Hagfeldt, M. Gratzel, Acc. Chem. Res. 33 (2000) 269.
[15] F. Pichot, B.A. Gregg, J. Phys. Chem. B 104 (2000) 6.
[16] S. Ito, P. Liska, P. Comte, R. Charvet, P. Péchy, U. Bach, L. Schmidt-Mende, S.M. Zakeeruddin, A. Kay, M.K. Nazeeruddin, M. Grätzel, Chem. Commun. (2005) 4351.
[17] B. Peng, G. Jungmann, C. Jäger, D. Haarer, H.-W. Schmidt, M. Thelakkat, Coord. Chem. Rev. 248 (2001) 1479.
[18] H. Tributsch, Appl. Phys. A: Mater. Sci. Process. 73 (2001) 305.
[19] M. Dürr, A. Yasuda, G. Nelles, Appl. Phys. Lett. 89 (2006) 061110.
[20] H. Nusbaumer, J.E. Moser, S.M. Zakeeruddin, M.K. Nazeeruddin, M. Grätzel, J. Phys. Chem. B 105 (2001) 10461.
[21] B.A. Gergg, F. Pichot, S. Ferrere, C.L. Fields, J. Phys. Chem. B 105 (2001) 1422.
[22] J.N. Hart, D. Menzies, Y.B. Cheng, G.P. Simon, L. Spiccia, C. R. Chimie 9 (2006) 622.
[23] R. Hattori, H. Goto, Thin Solid Films 515 (2007) 8045.
[24] P.K. Song, Y. Irie, S. Ohno, Y. Sato, Y. Shigesato, Jpn. J. Appl. Phys. 43 (2004) L442.
[25] M. Anpo, K. Chiba, J. Mol. Catal. 74 (1992) 207.
[26] J. Xia, N. Masakia, K. Jianga, S. Yanagida, J. Photochem. Photobiol. A 188 (2007) 120.
[27] J. Xia, N. Masaki, K. Jiang, S. Yanagida, J. Phys. Chem. C 111 (2007) 8092.
[28] M.F. Hossain, S. Biswas, T. Takahashi, Y. Kubota, A. Fujishima, J. Vac. Sci. Technol. A 26 (2008) 1012.
[29] G.K. Li, J.J. Shen, W.B. Mi, Z.Q. Li, P. Wu, E.Y. Jiang, H.L. Ba, Appl. Surf. Sci. 253 (2006) 425.
[30] A. Hauch, A. Georg, Electrochim. Acta 46 (2001) 3457.
[31] F. Fabregat-Santiago, J. Bisquert, G. Garcia-Belmonte, G. Boschloo, A. Hagfeldt, Sol. Energy Mater. Sol. Cells 87 (2005) 117.
[32] T. Hoshikawa, M. Yamada, R. Kikuchi, K. Eguchi, J. Electrochem. Soc. 152 (2005) E68.
[33] Q. Wang, J.E. Moser, M. Grätzel, J. Phys. Chem. B 109 (2005) 14945.
[34] A. Zaban, M. Greenshtein, J. Bisquert, ChemPhysChem 4 (2003) 859.
[35] F. Fabregat-Santiago, J. Bisquert, E. Palomares, L. Otero, D. Kuang, S.M. Zakeeruddin, M. Grätzel, J. Phys. Chem. C 111 (2007) 6550.
[36] J. Shu, J. Liang, S. Peng, W. Xu, J. Pei, J. Chen, Solid State Sci. 11 (2009) 433.